# Thermodynamics Drive Post-2016 Changes in the Antarctic Sea Ice Seasonal Cycle

Kenza Himmich, M. Vancoppenolle, Sharon Stammerjohn, Marion Bocquet, Gurvan Madec, Jean-Baptiste Sallée, Sara Fleury

JGR Oceans

RESEARCH ARTICLE
10.1029/2024JC021112

# Thermodynamics Drive Post-2016 Changes in the Antarctic Sea Ice Seasonal Cycle

**Kenza Himmich[1], Martin Vancoppenolle[1], Sharon Stammerjohn[2], Marion Bocquet[3,4], Gurvan Madec[1,5], Jean-Baptiste Sallée[1], and Sara Fleury[3]**

[1]Laboratoire d'Océanographie et du Climat, CNRS/IRD/MNHN, Sorbonne Université, Paris, France, [2]Institute of Arctic and Alpine Research, University of Colorado, Boulder, CO, USA, [3]LEGOS, CNES/CNRS/IRD/UPS, Université de Toulouse, Toulouse, France, [4]Collecte Localisation Satellites (CLS), Toulouse, France, [5]Inria, CNRS, Grenoble INP, LJK, Université Grenoble Alpes, Grenoble, France

**Abstract** Antarctic sea ice extent has been persistently low since late 2016, possibly owing to changes in atmospheric and oceanic conditions. However, the relative contributions of the ocean, the atmosphere and the underlying mechanisms by which they have affected sea ice remain uncertain. To investigate possible causes for this sea-ice decrease, we establish a seasonal timeline of sea ice changes following 2016, using remote sensing observations. Anomalies in the timing of sea ice retreat and advance are examined along with their spatial and interannual relations with various indicators of seasonal sea ice and oceanic changes. They include anomalies in winter ice thickness, spring ice removal rate due to ice melt and transport, and summer sea surface temperature. We find that the ice season has shortened at an unprecedented rate and magnitude, due to earlier retreat and later advance. We attribute this shortening to a winter ice thinning, in line with ice-albedo feedback processes, with ice transport playing a smaller role. Reduced ice thickness has accelerated spring ice area removal as thinner sea ice requires less time to melt. The consequent earlier sea ice retreat has in turn increased ocean solar heat uptake in summer, ultimately delaying sea ice advance. We speculate that the observed winter sea ice thinning is consistent with previous evidence of subsurface warming of the Southern Ocean.

**Plain Language Summary** Following 2016, the Antarctic sea ice cover has been persistently low. To understand why, we retrace the seasonal timeline of sea ice and oceanic changes, using satellite observations. We find that the sea ice season has been significantly shorter following 2016, due to a later start and an earlier end. This shortening is likely caused by thinner sea ice in winter, accelerating sea ice melt in spring and causing sea ice to disappear earlier. In turn, this has caused the ice-free ocean to absorb more solar heat in summer, and to take longer to cool down in the fall, ultimately delaying the ice season onset. Warmer waters beneath the Southern Ocean's surface, as evidenced by previous studies, could be a plausible cause of the observed thinning, by increasing the heat supply to sea ice.

**Key Points:**

- The Antarctic sea ice season duration has undergone an unprecedented shortening since 2016
- The changes include thinner ice, faster melt, earlier retreat, larger ocean heat uptake, later advance, in line with the ice-albedo feedback
- The near-circumpolar ice thinning suggests a possible increase in sensible heat supply by the ocean

**Supporting Information:**

Supporting Information may be found in the online version of this article.

**Correspondence to:**

K. Himmich,
kenza.himmich@locean.ipsl.fr

**Citation:**

Himmich, K., Vancoppenolle, M., Stammerjohn, S., Bocquet, M., Madec, G., Sallée, J.-B., & Fleury, S. (2024). Thermodynamics drive post-2016 changes in the Antarctic sea ice seasonal cycle. *Journal of Geophysical Research: Oceans*, *129*, e2024JC021112. https://doi.org/10.1029/2024JC021112

Received 26 MAR 2024
Accepted 30 JUL 2024
Corrected 21 SEP 2024

This article was corrected on 21 SEP 2024. See the end of the full text for details.

**Author Contributions:**

**Conceptualization:** Kenza Himmich
**Formal analysis:** Kenza Himmich, Martin Vancoppenolle
**Methodology:** Kenza Himmich
**Resources:** Marion Bocquet
**Supervision:** Martin Vancoppenolle, Sharon Stammerjohn, Gurvan Madec
**Writing – original draft:** Kenza Himmich
**Writing – review & editing:** Martin Vancoppenolle, Sharon Stammerjohn, Marion Bocquet, Gurvan Madec, Jean-Baptiste Sallée, Sara Fleury



## 1. Introduction

Antarctic sea ice has been subject to puzzling changes since the start of remote sensing observations. Over more than three decades, there was a striking contrast between the substantial decrease in Arctic sea ice (Cavalieri & Parkinson, 2012) and the overall weak but clear increase in Antarctic sea ice (Comiso, 2017; Parkinson & Cavalieri, 2012). In late 2016, however, Antarctic sea ice extent underwent an abrupt decline, sustained in the following years by several record lows (Parkinson, 2019; Raphael & Handcock, 2022).

The initial decrease in late 2016 has been mainly attributed to atmospheric processes. Anomalous winds produced by tropical teleconnections (Meehl et al., 2019) and a negative phase of the Southern Annular Mode (SAM; Schlosser et al., 2018; Turner et al., 2017) have warmed the surface ocean (Meehl et al., 2019) and limited the northward expansion of sea ice (Stuecker et al., 2017; Turner et al., 2017). By contrast, the sustained low sea ice state following 2016 has been attributed to both oceanic and atmospheric changes. Atmospheric changes include strengthened southward winds (Schroeter et al., 2023) and increased storm frequency (Turner et al., 2022). However, analyses of both climate model simulations (Mezzina et al., 2024; Zhang et al., 2022) and observations (Hobbs et al., 2024) suggest that atmospheric contributions alone are insufficient to explain the observed changes in sea ice. Instead, several studies point to a warming of the Southern Ocean subsurface as a key potential cause of the low sea ice state (Meehl et al., 2019; Purich & Doddridge, 2023; Zhang et al., 2022). Notably, the shift in the seasonal persistence of sea ice anomalies since 2010 (Hobbs et al., 2024; Purich & Doddridge, 2023), which is

linked to the vertical structure of oceanic properties (M. M. Holland et al., 2013; Libera et al., 2022), suggests that recent subsurface ocean and sea ice changes could be connected. Subsurface warming has been identified as a long-term response to a phase of negative Interdecadal Pacific Oscillation (IPO) and positive SAM, with resulting Ekman suction of warm subsurface waters (Ferreira et al., 2015; Kostov et al., 2017; Meehl et al., 2016). Northward sea ice transport induced by a positive SAM may have also contributed to this warming by increasing stratification and reducing subsurface ventilation (Haumann et al., 2020). Yet, how changes in atmospheric and oceanic conditions have affected sea ice remain unclear. Moreover, further evidence is required to establish the predominant role of subsurface warming over atmospheric processes in driving the recent sea ice changes.

Next to ice extent, useful markers of sea ice changes include the dates of advance and retreat, which represent two key transitions in the seasonal cycle of sea ice. Sea ice advance or retreat dates respectively mark the start and end of the sea ice season, defined as the first day in the year when sea ice concentration exceeds or falls below 15% (Massom et al., 2008; Stammerjohn et al., 2008). These two metrics allow for spatial analysis across the entire seasonal ice zone, and highlight which regions are changing, and which are not.

Changes in the timing of sea ice retreat can be traced back to prior ice thickness (Smith et al., 2020) whereas changes in sea ice advance relate to mixed layer heat content (Himmich et al., 2023). The heterogeneity of sea ice thickness, which varies up to meter scales (Thorndike et al., 1975), plays a crucial role in linking sea ice thickness to the following retreat date. Thinner ice at the satellite pixel scale (~25 km) implies a greater prevalence of subgrid-scale thin ice that melts more rapidly (M. M. Holland et al., 2006), leading to a faster sea ice concentration decrease and an earlier retreat. More subgrid-scale thin ice also promotes solar radiation uptake and basal melting (Maykut & McPhee, 1995; Maykut & Perovich, 1987; Vivier et al., 2016) further accelerating the decrease in sea ice concentration. In addition, earlier retreat increases solar radiation uptake (Perovich et al., 2007) and the mixed layer heat content during the open water season, delaying sea ice advance (Himmich et al., 2023; M. M. Holland et al., 2017; Stammerjohn et al., 2012). All these processes are expressions of the ice-albedo feedback. Ice transport also contributes to changes in sea ice seasonality by modifying the open water fraction (P. R. Holland & Kwok, 2012; M. M. Holland et al., 2017), intensifying or inhibiting the ice-albedo feedback (M. M. Holland et al., 2017; Massom et al., 2008; Stammerjohn et al., 2008). Examining changes in sea ice seasonality alongside changes in ice thickness, ocean heat content and ice concentration budget can therefore provide valuable insights into the drivers of the sea ice shift following 2016. However, changes in sea ice seasonality have only been documented until 2012, with large regional trends toward later retreat and earlier advance in the Amundsen and Bellingshausen Seas and, earlier retreat and later advance in the Ross Sea (e.g., Simpkins et al., 2013). Possible shifts in sea ice seasonality following 2016 have yet to be investigated.

In this study, we evaluate the changes in sea ice seasonality following 2016, based on passive microwave sea ice concentration records. We analyze possible drivers of these changes, including ice-albedo feedback processes and ice transport, using satellite observations of sea ice thickness, sea surface temperature, ice concentration budget diagnostics, and an idealized sea ice model. Finally, we discuss whether those changes point to the atmosphere or the ocean as the key driver of the recent sea-ice shift.

## 2. Data

This study is based on satellite observations of sea ice concentration, drift, thickness and sea surface temperature. We use daily passive microwave sea ice concentration over 1979–2022 (EUMETSAT Ocean and Sea Ice Satellite Application Facility, 2022a, 2022b; Lavergne et al., 2019) and sea ice drift over 1991–2020 (EUMETSAT Ocean and Sea Ice Satellite Application Facility, 2022c; Lavergne & Down, 2023) from EUMETSAT Ocean and Sea Ice Satellite Application Facility (OSI-SAF), with respective resolutions of 25 and 75 km. Fields of sea ice drift are retrieved using different methods according to the season. In winter, from April to September, ice drift is retrieved using a maximum cross correlation algorithm applied to brightness temperature from a number of sensors (SSM/I, SSMIS, AMSR-E, and AMSR2). In summer, from November to February, a free-drift model based on the ERA5 wind fields is used (Hersbach et al., 2020). In October and March, the fields are derived from both model and satellite-based outputs.

For sea ice thickness, we utilized altimetry-based ice thickness retrievals from 1994 to 2022, as provided by Bocquet and Fleury (2023). This data set integrates year-round 12.5 km gridded radar freeboard time series from ERS-1, ERS-2, Envisat, and CryoSat-2 missions. Different missions are inter-calibrated, leveraging mission

overlap. Ku-band radar echoes are corrected for the varying speed of light in snow (Mallett et al., 2020) and converted to radar freeboards following the methodology outlined by Laxon et al. (2003). The density of ice (875–920 kg/m³) and snow (320–350 kg/m³) includes specified seasonal variations (Kurtz & Markus, 2012; Maksym & Markus, 2008). To retrieve ice thickness, an ensemble of snow depth products is employed—including radiometer- and altimetry-based climatologies (Garnier et al., 2021; Paul et al., 2021), alongside radiometer-based interannual estimations (Comiso et al., 2003; Markus & Cavalieri, 1998; Meier, 2017). Using these snow depth products and the radar freeboard, multiple thickness estimates are derived based on the equilibrium equation for snow-covered sea ice. The final ice thickness product is determined as the ensemble mean of all estimates. A detailed evaluation was conducted by Bocquet (2023) against various in situ sources—the ASPeCt visual observations (Worby et al., 2008), ice draft from upward-looking sonars on AWI moorings in the WtNOTIMeddell Sea (Behrendt et al., 2013)—and against airborne altimetry from Operation Ice Bridge (Kurtz et al., 2013). This evaluation revealed significant differences with regional and temporal variations rather than systematic biases, and indicated that the thickness time series are in reasonable agreement with observations.

Finally, we use a daily satellite product of sea surface temperature available over 1982–2022, based on thermal infra-red radiance measurements, and taken from the global L4 (gap-free, gridded) European Space Agency (ESA) SST Climate Change Initiative (CCI) analysis with a resolution of 0.05° (Copernicus Climate Change Service (C3S), 2019; Merchant et al., 2019).

All data are either interpolated on the OSI-SAF Equal-Area Scalable Earth 2 (EASE2) 25 or 75 km grid.

## 3. Methods

### 3.1. Sea Ice Concentration Budget

To unravel the thermodynamic and dynamic nature of the processes contributing to the recent sea ice changes, we use a sea ice concentration budget decomposition based on the governing equation for sea ice concentration ($C$; P. R. Holland & Kwok, 2012):

$$\frac{\partial C}{\partial t} = -\nabla.(uC) + \text{residual} \tag{1}$$

$$\nabla.(uC) = u.\nabla C + C\nabla.u \tag{2}$$

here $u$ is the sea ice drift field. The dynamic term ($\nabla.(uC)$) represents advection ($u.\nabla C$) and divergence ($C\nabla.u$) of sea ice caused by ice drift whereas the residual term includes both thermodynamic processes (melting/freezing) and mechanical redistribution (ridging/rafting).

We apply the methodology of P. R. Holland and Kimura (2016) on OSI SAF sea ice concentration and drift data to compute the dynamic and residual contributions to the budget. Sea ice concentration fields are interpolated on the 75-km grid of ice drift. A $7 \times 7$ cell square-window smoothing filter is then applied to the ice drift fields in order to avoid noise in the dynamic term. The time derivative in ice concentration is calculated as a central difference in time of sea ice concentration fields at a daily frequency. Advection and divergence terms are calculated as central differences in space then averaged over 3-day periods to synchronize with time derivatives.

### 3.2. Diagnostics of Sea Ice and Sea Surface Changes

For each year of available observational records, we establish a seasonal timeline of potential sea ice and sea surface changes using the diagnostics summarized in Figure 1. We consider that each year starts and ends in September, during the ice season. For example, 1980 starts on 15th September 1979 and ends in 14th September 1980.

To diagnose the changes in sea ice seasonality, we derived the dates of sea ice retreat and advance from satellite sea ice concentration, on which we previously applied a 15-day temporal filter to exclude any date reflecting short events (Lebrun et al., 2019). The date of retreat is defined as the first day filtered sea ice concentration drops below 15% while the date of advance is the first day filtered sea ice concentration exceeds 15%, similar to previous studies (Lebrun et al., 2019; Parkinson, 1994; Simpkins et al., 2013; Stammerjohn et al., 2012). We searched for dates of advance starting on January 1st, a month where no sea ice advance occurs, on average over

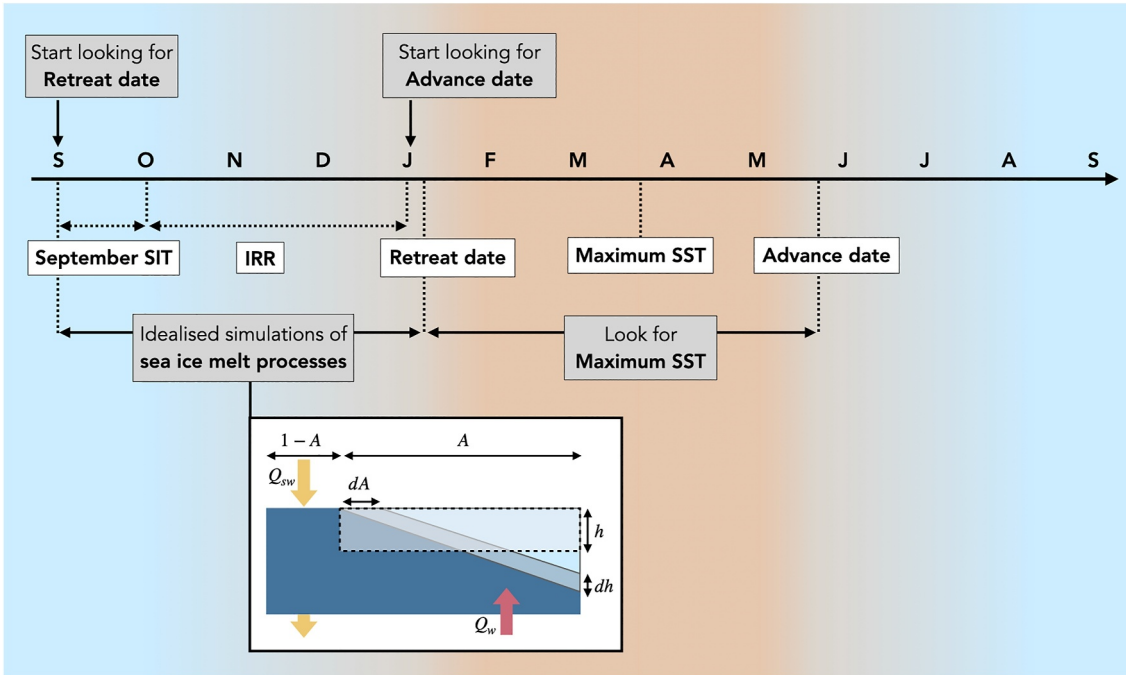


**Figure 1.** Schematic view of the sea ice diagnostics and idealized model used in this study. The diagnostics include: mean September sea ice thickness (SIT), Ice Removal Rate (IRR, the average loss rate of ice concentration over the melt season), retreat date, seasonal maximum of sea surface temperature (SST) and advance date. Diagnostics are evaluated for each year and pixel, whereas the model focuses on the melt season.

1980–2022. We then looked for the prior dates of retreat occurring between September 15th and corresponding dates of advance.

To diagnose possible changes during the ice and open water seasons, we respectively use sea ice thickness and sea surface temperature. Sea ice thickness is averaged over the leading September month, representing the end-of-winter thickness, close to the seasonal maximum. For each year, we also search for the seasonal maxima of sea surface temperature, between the retreat date and the next advance date.

To investigate the changes in spring ice removal processes possibly leading to changes in the retreat dates, we define the spring (over October, November, and December) sea ice removal rate (IRR) as:

$$\mathrm{IRR} = -\int_{\mathrm{OND}} \frac{\partial C}{\partial t}_{<0} dt \tag{3}$$

The IRR filters the positive derivatives to ensure focus on removal processes. Using the sea ice concentration budget decomposition, we also calculated the dynamic and residual contributions to the IRR for each year over 1992–2020. Climatological fields of IRR and contributions show that the dynamic term is positive in the inner sea ice zone due to ice export out of that inner zone and negative in the outer sea ice zone due to ice import into that outer zone (see Figure S1 in Supporting Information S1). This dynamic contribution is, however, small compared to the residual, which dominates the removal rate over all the seasonal ice zone. Based on these considerations, positive (negative) anomalies in IRR can be interpreted as an increase (decrease) in ice removal. Positive (negative) anomalies in dynamic contribution would suggest increased (decreased) ice export in the inner pack and decreased (increased) ice import in the outer pack. Interpreting the sign of anomalies in residuals is not as straightforward because it accounts for both melt and mechanical redistribution processes.

For any statistical calculations conducted in this study involving the previously mentioned diagnostics, a missing value is assigned where the number of years with undefined retreat or advance dates (corresponding to year-round ice-free or ice-covered grid points) is less than one third of the total number of years in the considered period,

following Lebrun et al. (2019). This procedure ensures that meaningful and consistent averages, trends or correlations are obtained.

Due to varying time periods of data availability (see Section 2), statistical analyses were conducted over slightly different time periods for the different diagnostics (1980–2022; 1983–2022; 1995–2022; or 1992–2020), and adapted accordingly. We controlled this inconsistency had as little influence as possible (see Figure S2 in Supporting Information S1).

### 3.3. Idealized Model Simulations of Spring Sea Ice Decay

To explore the thermodynamic mechanisms linking changes in sea ice thickness to changes in the following spring IRR and retreat date, we performed idealized model simulations of the spring sea ice decay. Our model encapsulates physics of sea ice melting, in particular the effect of the ice-albedo feedback on basal melting. The ice-albedo feedback is here viewed in the sense of M. M. Holland et al. (2006) and describes how solar radiation uptake amplifies a small change in ice concentration by promoting basal melt of thin ice, further reducing ice coverage.

We consider a given ice-covered region of the ocean (e.g., a satellite pixel), characterized by ice concentration $A(t)$ and mean thickness $h(t)$, and a surface ocean layer of constant thickness $h_w = 20$ m (Figure 1). External heat inputs to the surface ocean-sea ice system are net solar radiation uptake and sensible ocean heat flux. The surface ocean layer temperature is fixed at the freezing point, so that any heat absorbed in the surface layer is converted into basal melt. This approach was introduced in large-scale sea ice models by Fichefet and Morales Maqueda (1997) and Häkkinen and Mellor (1990) and is known to provide a sensible first-order emulation of the ice thickness distribution.

Net solar radiation uptake in the ocean surface layer (W/m$^2$) results from the balance of incident, absorbed and transmitted solar radiation, assuming absorption of most solar radiation in a thin surface layer and exponential attenuation with depth (Lengaigne et al., 2007):

$$Q_{sw} = Q_{sw}^{\downarrow}(1-\alpha_w)\cdot[1-(1-R)\cdot\exp(-\kappa h_w)]. \tag{4}$$

$Q_{sw}^{\downarrow}$ is the incident solar radiation (W/m$^2$), $\alpha_w = 0.06$ is the ocean albedo, $R = 0.58$ is the fraction of solar radiation absorbed in a small (~10 cm) surface layer and $\kappa = 1/23$ m$^{-1}$ is the bulk solar attenuation coefficient.

Ice thickness $h$ decreases due to a prescribed sensible heat flux $Q_w$ and net solar radiation uptake in the surface layer:

$$-\rho L\cdot\frac{dh}{dt} = Q_w + p_1\cdot Q_{sw}\cdot\left(\frac{1-A}{A}\right), \tag{5}$$

where $\rho = 917$ kg/m$^3$ is the ice density and $L = 335{,}000$ J/kg is the latent heat of fusion. The $(1-A)/A$ factor reflects heat conservation: solar radiation penetrates through the open water fraction $(1-A)$ and is attributed over the ice-covered fraction $A$ of the grid cell.

The ice concentration loss rate depends on the subgrid scale ice thickness distribution, and is in particular controlled by the melt rate of thin ice (M. M. Holland et al., 2006). Here we assume that the ice thickness is homogeneously distributed between zero and twice the mean. In this context, a decrease in mean thickness implies a loss of thin ice, and the ice concentration decreases as follows:

$$\frac{dA}{dt} = p_2\cdot\frac{A}{2h}\cdot\frac{dh}{dt}. \tag{6}$$

We also introduce two parameters $p_1$ and $p_2$ ([0,1]) that tune solar radiation uptake and the loss of concentration per unit ice thickness (which depends on the ice thickness distribution, unresolved here).

We run simulations with varying $h_{max}$ from 0.5 to 2.5 m. All simulations span 150 days of sea ice melting, starting with maximum thickness $h_{max}$ and initial ice concentration $A_{max} = 0.99$. The sensible heat flux $Q_w$ is assumed constant, with a representative value of 30 W/m$^2$. Solar radiation linearly increases from 50 to 250 W/m$^2$ from day

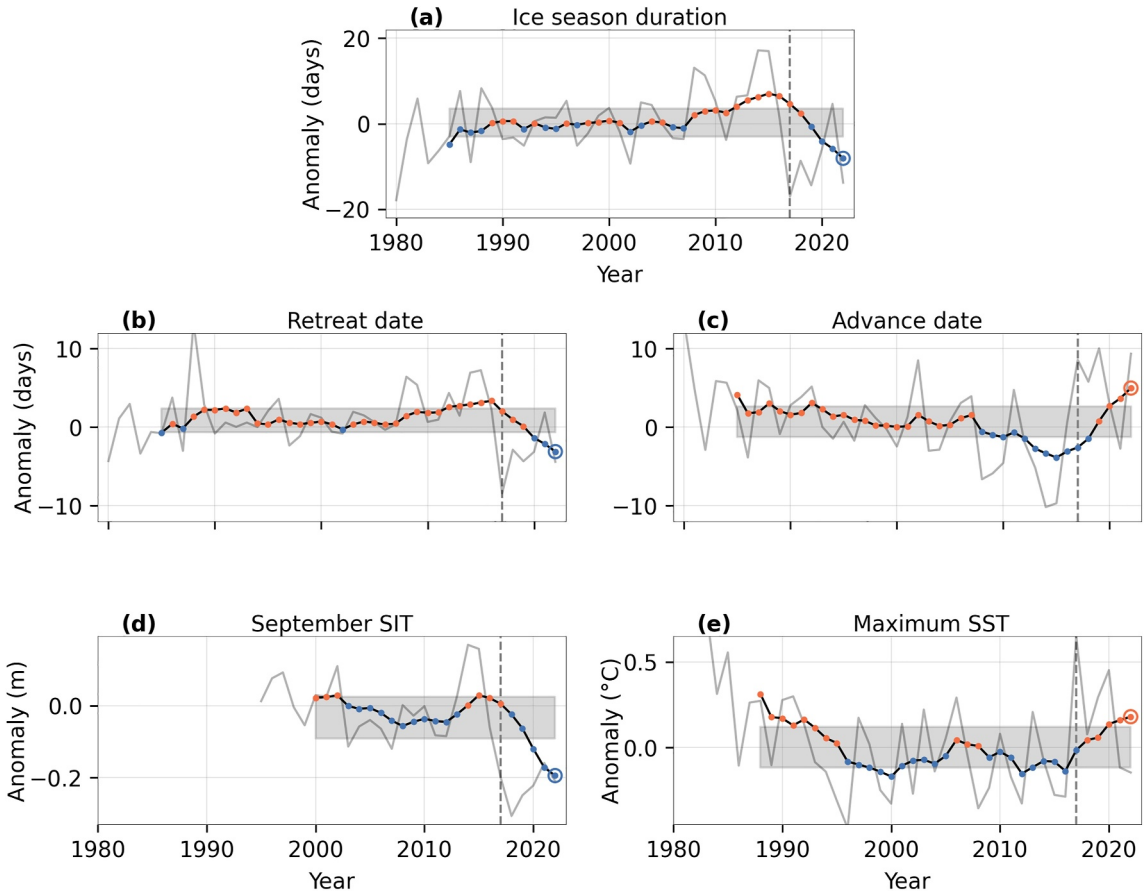


**Figure 2.** Time series of selected sea ice and ocean diagnostics. Gray solid lines show yearly anomalies in (a), ice season duration, (b), retreat dates, (c), advance dates, in (d), September sea ice thickness (SIT) and (e), maximum sea surface temperature (SST). Yearly anomalies represent spatial mean differences over the seasonal ice zone of annual 2D fields with respect to the mean 2D field over pre-2016 period. The reference period depends on data availability: 1980–2016 for (a–c); 1995–2016 for (d) and 1983–2016 for (e). Black lines with colored dots show 6-year running mean anomalies such that the last point represents the spatial mean of the 2D fields depicted in Figure 3. Red dots mark positive values whereas blue dots mark negative values. Stippled gray lines mark 2017. The gray areas delimit the mean ± the standard deviation of 6-year running mean anomalies over the whole time series.

1 to day 150, which is representative of the Antarctic sea ice zone from September to December (Vancoppenolle et al., 2011). Three ensembles are run. In the control ensemble, both shortwave enhancement and ice concentration loss are active ($p_1 = p_2 = 1$). They are switched off separately in the two other ensembles.

The simulations feature a rapid ice concentration and thickness loss, and achieve complete ice decay within a few weeks. From each simulation, we diagnose the average IRR as the mean of $dA/dt$ over the whole simulation period, and the retreat date as the last day of simulation with $A > 15\%$.

## 4. Unprecedented Shortening of the Sea Ice Season Following 2016

We analyze post-2016 changes in ice season duration, retreat, and advance dates in relation to the pre-2016 period. Potential shifts in long-term trends as well as the spatial extent, magnitude and rate of these changes are examined based on various analyses.

Yearly anomalies in ice season duration, retreat and advance dates indicate a significant shift following 2016 (Figure 2, gray line). Over 1980–2016, the sea ice season duration shows a clear increase of 3.6 days per decade (Figure 2a; Table 1) due to trends toward 1 day later retreat and 2.6 days earlier advance per decade (Figures 2b and 2c). Over 2016–2017, however, an abrupt shortening occurs, followed by large negative anomalies maintaining the ice season duration at low values until 2022 (Figures 2a–2c). As a result of this reversal in behavior after 2016, the ice duration trend over 1980–2022 is small and not statistically significant (Table 1). The weakening of circumpolar trends results from regional pattern changes, evident when comparing regional trends

**Table 1**
*Long-Term Trends in Selected Sea Ice and Ocean Diagnostics*

| | Trends ending in 2016 | Trends ending in 2022 |
|---|---|---|
| Ice season duration (days/dec.) 1980–2022 | **3.6 ± 1.0*** | 0.6 ± 1.0 |
| Retreat date (days/dec.) 1980–2022 | **1.0 ± 0.5*** | −0.2 ± 0.5 |
| Advance date (days/dec.) 1980–2022 | **−2.6 ± 0.6*** | −0.8 ± 0.6 |
| September SIT (cm/dec.) 1995–2022 | −0.3 ± 3 | **−8.0 ± 2.0*** |
| Maximum SST (°C/dec.) 1983–2022 | **−0.15 ± 0.04*** | −0.06 ± 0.04 |

*Note*. Trends are defined as the linear least square fit slopes for the yearly anomalies, averaged over the seasonal ice zone, over time periods ending either in 2016 or in 2022. Time periods are chosen according to underlying data availability and are indicated in the first column of the table. Slopes standard errors are given as uncertainties. Asterisks indicate statistically significant trends at the 95% level.

over 1980–2022 and 1980–2016 (see Figure S3 in Supporting Information S1). The largest regional trends toward a longer ice season prior to 2017, located in the Ross and Weddell Seas, have weakened over 1980–2022. Additionally, significant trends toward a shorter ice season have emerged in the Bellingshausen Sea and the Indian sector over 1980–2022.

Spatial patterns of post-2016 changes in ice season length align consistently with the weakening of regional trends (Figure 3a). Based on the 6-year mean anomaly over 2017–2022 referenced to the pre-2016 period, we find that

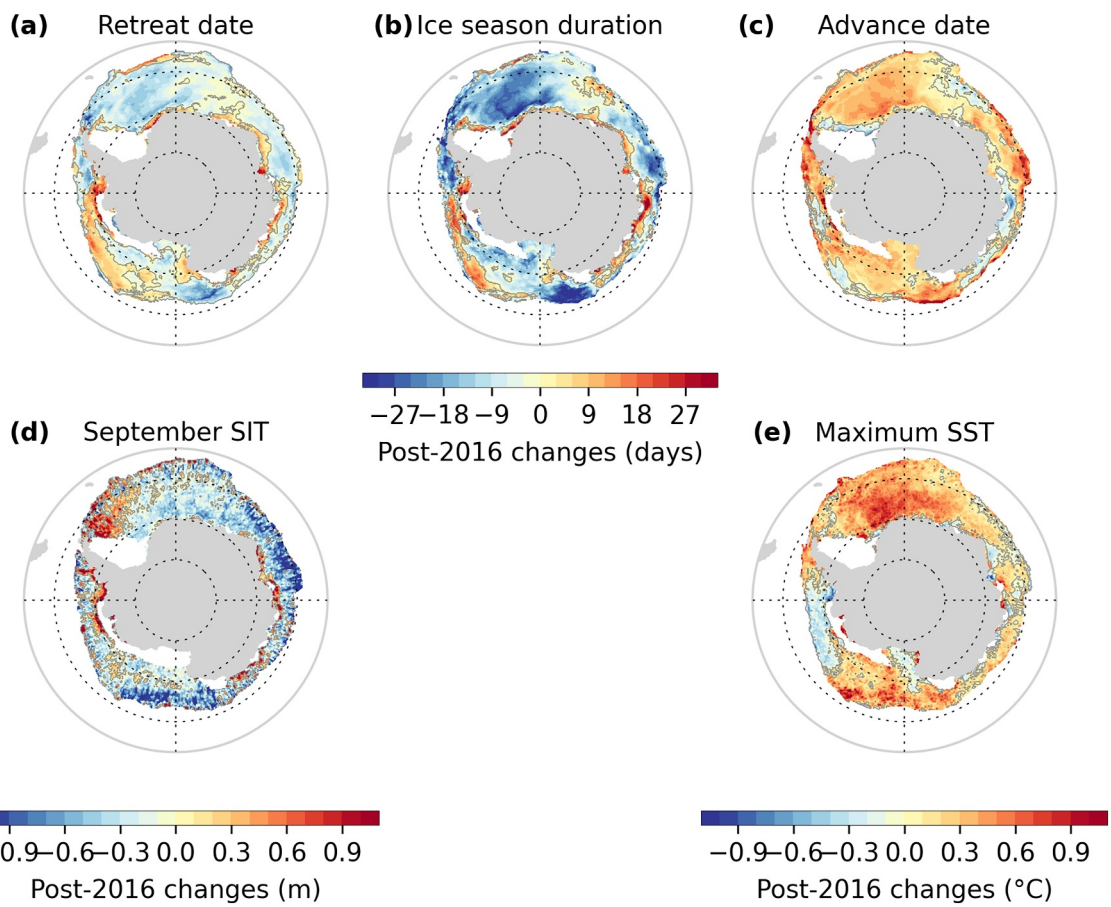


**Figure 3.** Post-2016 changes in (a), retreat date, (b), advance date, (c), ice season duration, (d), September sea ice thickness (SIT) and (e) maximum sea surface temperature (SST). Changes are calculated as differences between the 2017–2022 mean 2D fields and their pre-2016 counterpart. The reference period for pre-2016 conditions depends on data availability: 1980–2016 for (a–c); 1995–2016 for (d) and 1983–2016 for (e). White patches indicate regions out of the seasonal ice zone.

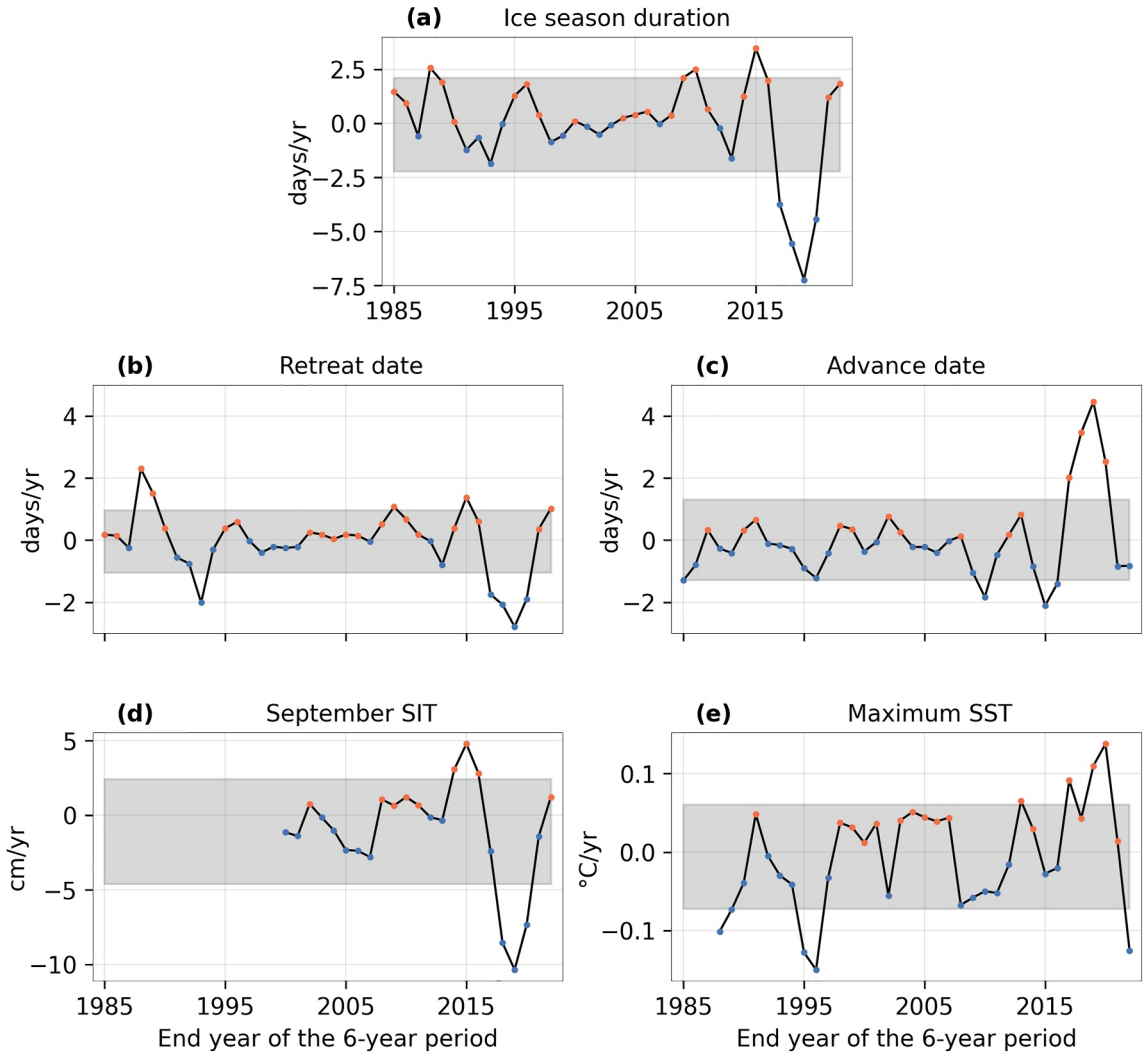


**Figure 4.** Rate of 6-year changes in selected sea ice and ocean diagnostics. Rates are calculated as least-square slopes over 6 years of yearly anomalies in (a), ice season duration, (b), retreat date, (c), advance date (d), September sea ice thickness (SIT), and (e), maximum of sea surface temperature (SST). Yearly anomalies represent spatial mean differences over the seasonal ice zone of annual 2D fields with respect to the mean 2D field over pre-2016 period. The reference period depends on data availability: 1980–2016 for (a–c); 1995–2016 for (d) and 1983–2016 for (e). Blue dots mark negative values whereas red dots mark positive values. The gray areas delimit the mean ± the standard deviation over the whole time series.

the ice season shortening is overall circumpolar, but largest in the Ross, Bellingshausen, Weddell and Indian sectors. These spatial patterns are weakly sensitive to the choice of the calculation period (see Figure S2 in Supporting Information S1), and remain similar for all 4 periods considered in the study (see Section 3).

We next compare the magnitude and rate of the post-2016 ice season shortening to previous 6-year changes. On average over the seasonal ice zone (Figures 3a–3c), the ice season is 8.9 days shorter over 2017–2022 compared to 1980–2016, due to 3.7 days earlier retreat and 5.2 days later advance. Based on 6-year running mean anomalies over 1980–2022, we find that these changes are larger than any previous 6-year changes (Figures 2a–2c, black lines). Specifically, the 2017–2022 mean anomaly in ice season duration is the lowest on record, being 2 days shorter than the previous shortest ice season 6-year mean anomaly (2016–2021) and exceeding three times the standard deviation (Figure 2a). The 2017–2022 mean anomaly is also record breaking for both retreat and advance dates by approximately 1 day (Figures 2b and 2c). In addition, the post-2016 changes in sea ice seasonality are unusually rapid, with rates of change over 6-year periods ending after 2017 exceeding those of earlier periods and the standard deviation (Figures 4a–4c). The fastest 6-year changes in retreat and advance dates over the entire time series occur over 2013–2019 (i.e., ending in 2019, as shown in Figures 4b and 4c), reaching respectively

more than 2 times and 3 times the standard deviation. These findings indicate that the earlier retreat, later advance and consequent shorter sea ice season following 2016 have an unprecedented magnitude and rate within the satellite record.

Hence, due to a near-circumpolar shortening following 2016, the evolution of sea ice season duration over 1980–2022 closely parallels the changes observed in ice extent, with a long-term increase followed by an unprecedentedly large and rapid decrease in 2017, as shown by Parkinson (2019).

## 5. Drivers of the Recent Sea Ice Season Shortening

### 5.1. Shorter Ice Season: Response to Ice Thinning?

We hypothesize that the ice season shortening following 2016 might be tied to changes in ice thickness and upper ocean heat content. Accordingly, in this section, we examine the changes in the September sea ice thickness over 1995–2022 and in the seasonal maximum of sea surface temperature, used as a proxy of the summer mixed layer heat content (Himmich et al., 2023), over 1983–2022.

Similar to retreat and advance dates, September ice thickness and maximum sea surface temperature have undergone unprecedented changes since 2016. Long-term trends in these variables have shifted noticeably around 2016 (Table 1). Over 1995–2016, sea ice thickness exhibits no statistically significant trend, while over 1995–2022, a statistically significant trend emerges, showing a decrease of 8 cm per decade. A shift is also observed for sea surface temperature in 2016. Over 1983–2016, maximum sea surface temperature anomalies exhibit a statistically significant trend toward colder sea surface temperatures by 0.15°C per decade. However, over 1983–2022, the trend becomes almost nil. This shift in long-term trends stems from large yearly anomalies toward thinner sea ice and warmer sea surface temperature occurring after 2016 (Figures 2d and 2e, gray lines), at unprecedented magnitude and rate. Notably, the mean anomaly over 2017–2022 is the lowest on record for thickness and the second highest on record for temperature, among 6-year mean anomalies (Figures 2d and 2e, black lines). Moreover, the fastest sea ice thinning and sea surface warming among rates of change over 6-year occur after 2017, respectively ending in 2019 and 2020 (Figures 4d and 4e).

The coinciding earlier retreat, later advance, thinner sea ice and warmer sea surface temperatures suggest that these changes could be linked. That the post-2016 ice thinning and sea surface warming occur mainly where the changes in retreat and advance dates are the largest supports this hypothesis (Figure 3; see Figure S2 in Supporting Information S1). Based on 6-year mean anomalies over 2017–2022 referenced to the pre-2016 period, we find that 72% of seasonal ice zone grid points with earlier retreat spatially correspond to thinner September sea ice. Earlier retreat due to thinning reflects either a thermodynamic response, with increased melt rate, or a dynamic response, with increased sensitivity to transport, as suggested by M. M. Holland et al. (2006). This point will be further investigated in the next section. We also find that 85% of the grid points with higher maximum sea surface temperature also show an early retreat. In turn, 92% of grid points with later advance have a higher sea surface temperature. The correspondence between earlier retreat, warmer sea surface temperature and later advance is consistent with ice-albedo feedback processes during the open water season (Himmich et al., 2023; M. M. Holland et al., 2017; Manabe & Stouffer, 1980; Stammerjohn et al., 2012): earlier retreat increases solar heat uptake into the mixed layer; the extra heat needs more time to be released, which delays sea ice advance. Accordingly, 77% of the grid points with later sea ice advance also have earlier ice retreat. Hence, reduced winter thickness is a probable factor causing the early retreat, increased summer ocean heat content, and late advance following 2016.

Yearly anomalies follow a consistent sequence of processes, supporting the causality of the previous links. For instance, in 2017, the anomalously low September sea ice thickness comes first in order, followed by the earlier retreat, warmer maximum sea surface temperature and ultimately, later advance (Figure 2, gray lines). Further evidence of causality is provided by correlating the mean detrended anomalies averaged over the seasonal ice zone from the 1995–2022 time series. This specific period was selected due to the availability of relevant diagnostics. We observe a statistically significant link ($R^2 = 0.34$, $p < 0.01$) between the mean September sea ice thickness and the subsequent mean retreat date (Figure 5a). This relationship indicates that for each centimeter of ice thinning, the retreat occurs 0.22 days earlier. We also observe a statistically significant link between retreat and subsequent advance date anomalies ($R^2 = 0.75$, $p < 0.01$), indicating a delay in advance of 1.3 days per day of early retreat (Figure 5b). The link between anomalies in retreat date and subsequent maximum sea surface

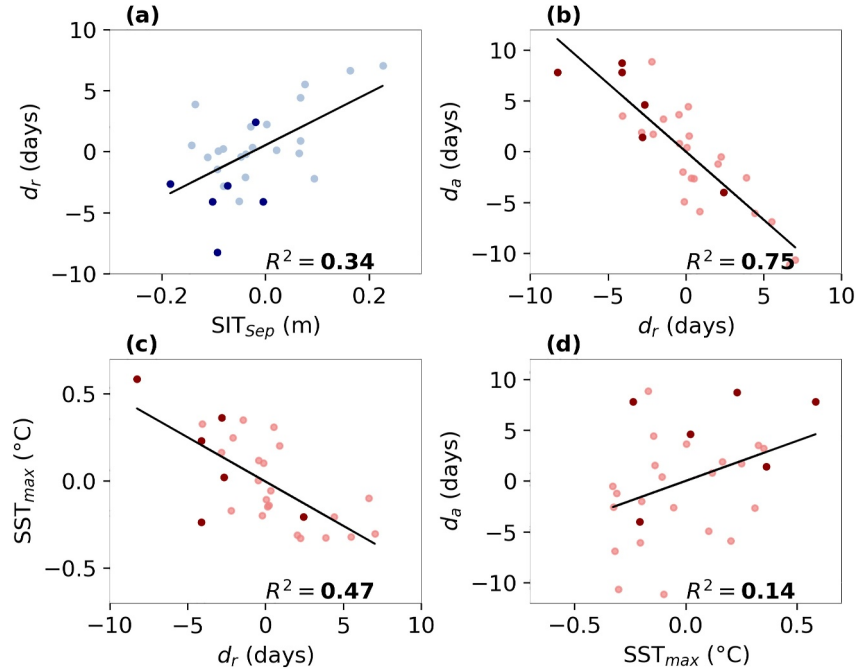


**Figure 5.** Interannual relationships between selected sea ice and ocean diagnostics, over 1995–2022. Detrended yearly anomalies, averaged over the seasonal ice zone, of (a), retreat dates ($d_r$) versus September sea ice thickness (SIT$_{Sep}$), (b), advance dates ($d_a$) versus $d_r$, (c), maximum sea surface temperature (SST$_{max}$) versus $d_r$, (d), $d_a$ versus SST$_{max}$. Blue tones indicate ice season relations whereas red tones indicate open water season relations, as illustrated in this figure. 2017–2022 anomalies are marked in dark colors. A Least Square linear regression was performed for each plot; the corresponding regression line (significant at 99%), and corresponding coefficients of determination ($R^2$) are shown. The 1995–2022 period was selected to ensure consistency of the analysis, as all relevant diagnostics are available over this timeframe. Positive $d_r$ ($d_a$) indicates later retreat (advance) while negative $d_r$ ($d_a$) indicates earlier retreat (advance).

temperature appears relatively strong ($R^2 = 0.47$, $p < 0.01$; Figure 5c), when compared with the link between maximum sea surface temperature and subsequent advance date ($R^2 = 0.14$, $p < 0.01$; Figure 5d). We argue this reflects the importance of accounting for mixed layer depth to accurately evaluate the mixed layer heat content when the ocean is cooling down during open water season (Himmich et al., 2023). The maximum sea surface temperature is potentially a better proxy of the mixed layer heat content during the warming period, due to shallower mixed layers, explaining why the temperature is more strongly linked to retreat dates than to advance dates.

Based on these spatial and interannual linkages (see Figure 6), we surmise that the decrease in the September ice thickness has contributed to the earlier sea ice retreat following 2016. This has, in turn, lead to a warming of the upper ocean and delayed sea ice advance through the ice-albedo feedback. However, whether the earlier retreat is a result of thermodynamic or dynamic changes remains to be established.

### 5.2. Earlier Retreat: A Dynamic or Thermodynamic Response to Ice Thinning?

To unravel the thermodynamic or dynamic nature of the relationship between ice thinning and early retreat, we examine melt season processes based on a sea ice concentration budget derived from passive-microwave concentration and drift. We evaluate the average sea ice area removal rate (IRR) over spring (October, November, December) as well as the dynamic and residual contributions to the IRR, over 1992–2020. The dynamic contribution to the IRR is mostly due to the northward export of sea ice (see Figure S1 in Supporting Information S1) whereas residuals include both melting and, also, to some extent, mechanical redistribution through ridging and rafting (P. R. Holland & Kimura, 2016).

We find that the post-2016 shift is also seen in the spring ice removal processes. Yearly IRR anomalies decrease to lower than average values over 1992–2016, then undergo an unprecedentedly rapid rise (see Figure S4 in Supporting Information S1), starting in the spring before the early ice retreat of 2017 (Figure 7a, gray line). The

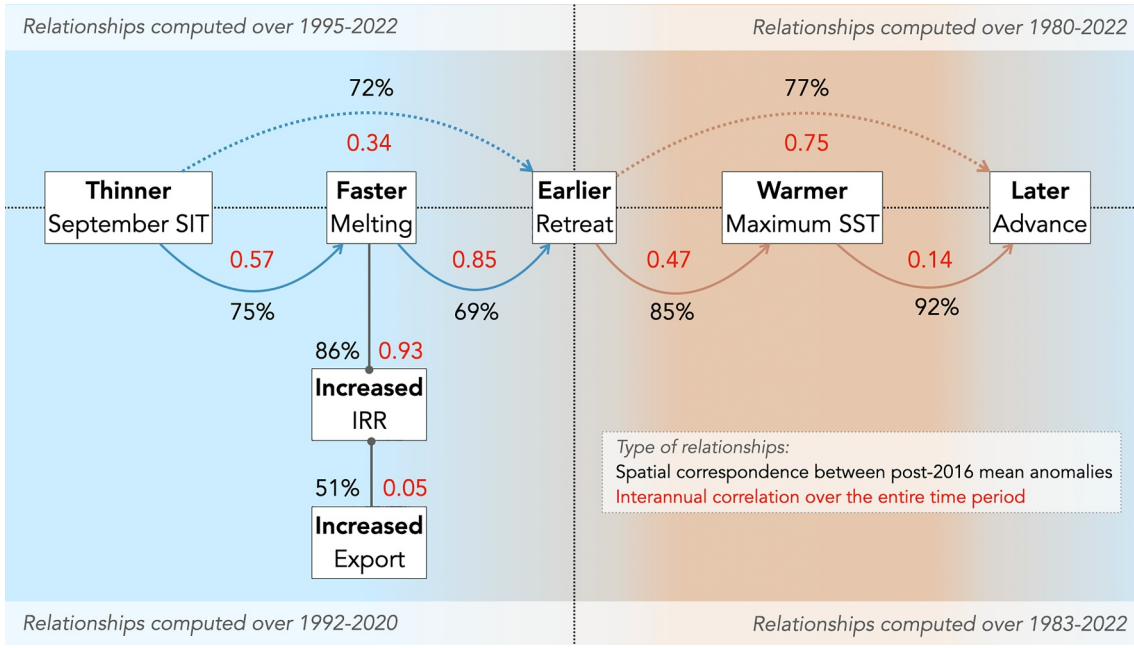


**Figure 6.** Schematic of the thermodynamic response of sea ice and sea surface temperature (SST) to a reduction in ice thickness (SIT). Colored lines represent ice-albedo feedback processes occurring within the sea-ice season (blue) versus open water season (orange). Gray lines represent the dynamic and thermodynamic contributions to the ice removal rate (IRR). Red numbers refer to the coefficient of determination ($R^2$) of interannual correlations between the considered variables, as shown in Figures 5 and 8. Percentages quantify the spatial correspondence between the post-2016 changes in specified variables, based on mean anomalies (see Figures 3 and 7; Figure S2 in Supporting Information S1). The time period considered for each spatial relationship, which depends on underlying data availability, is specified on the schematic.

magnitude of this post-2016 increase is also unusually large, with the mean anomaly over 2017–2020 ranking as the second largest among previous 4-year mean anomalies (Figure 7a, black line). Yearly anomalies in the residual contribution to the IRR evolve similarly (Figure 7c, gray line) and account for 93% of the interannual variance in total IRR (Figure 8a). Conversely, anomalies in the dynamic contribution show comparatively small variations (Figure 7e, gray line) and only explain 5% of the variance in total IRR (Figure 8b).

Residuals thus appear to be the major contributor to the recent increase in IRR compared to sea ice export. This is also highlighted by similar spatial patterns of post-2016 changes in IRR and residual contribution (Figures 7b and 7d), calculated as the mean anomaly over 2017–2020 referenced to the period pre-2016. Notably, 86% of the seasonal ice zone grid points with increased IRR correspond to increased residual contribution. By contrast, substantial spatial discrepancies are observed between the mean anomalies in IRR and in the dynamic contribution (Figures 7b and 7f). Furthermore, the absence of ice thickening in spring (see Figure S5 in Supporting Information S1) in regions of increased residual contribution (Figure 7d) suggests that ridging and rafting weakly contribute to the IRR, and that thermodynamics must dominate the increase. Hence, the post-2016 IRR increase is likely caused by a more rapid melt-back.

The post-2016 increase in residual IRR is also related to changes in September sea ice thickness and retreat date. We find that 75% of grid points showing an increase in residual IRR (Figure 7d) correspond to thinner sea ice (Figure 3d). Additionally, 69% of grid points with early retreat (Figure S2 in Supporting Information S1) correspond to increased residual contribution (Figure 7d). The same links are also evident at interannual time scales, reinforcing the credibility of causality. Detrended anomalies in September sea ice thickness explain 57% of the interannual variance in residual IRR in the following spring (Figure 8c). In turn, mean detrended anomalies in residual IRR explain 85% of the variance in the following retreat dates (Figure 8d). These findings suggest that the earlier retreat observed post-2016 is likely a thermodynamic response to ice thinning, which has led to increased residual IRR due to enhanced sea ice melt (see Figure 6).

Idealized model simulations of spring sea ice melt (see Section 3) provide further support for and understanding of this thermodynamic response. The control simulation ensemble features links between maximum thickness, IRR and retreat date that are similar to observations (Figure 9). The simulated relationships are roughly linear over the

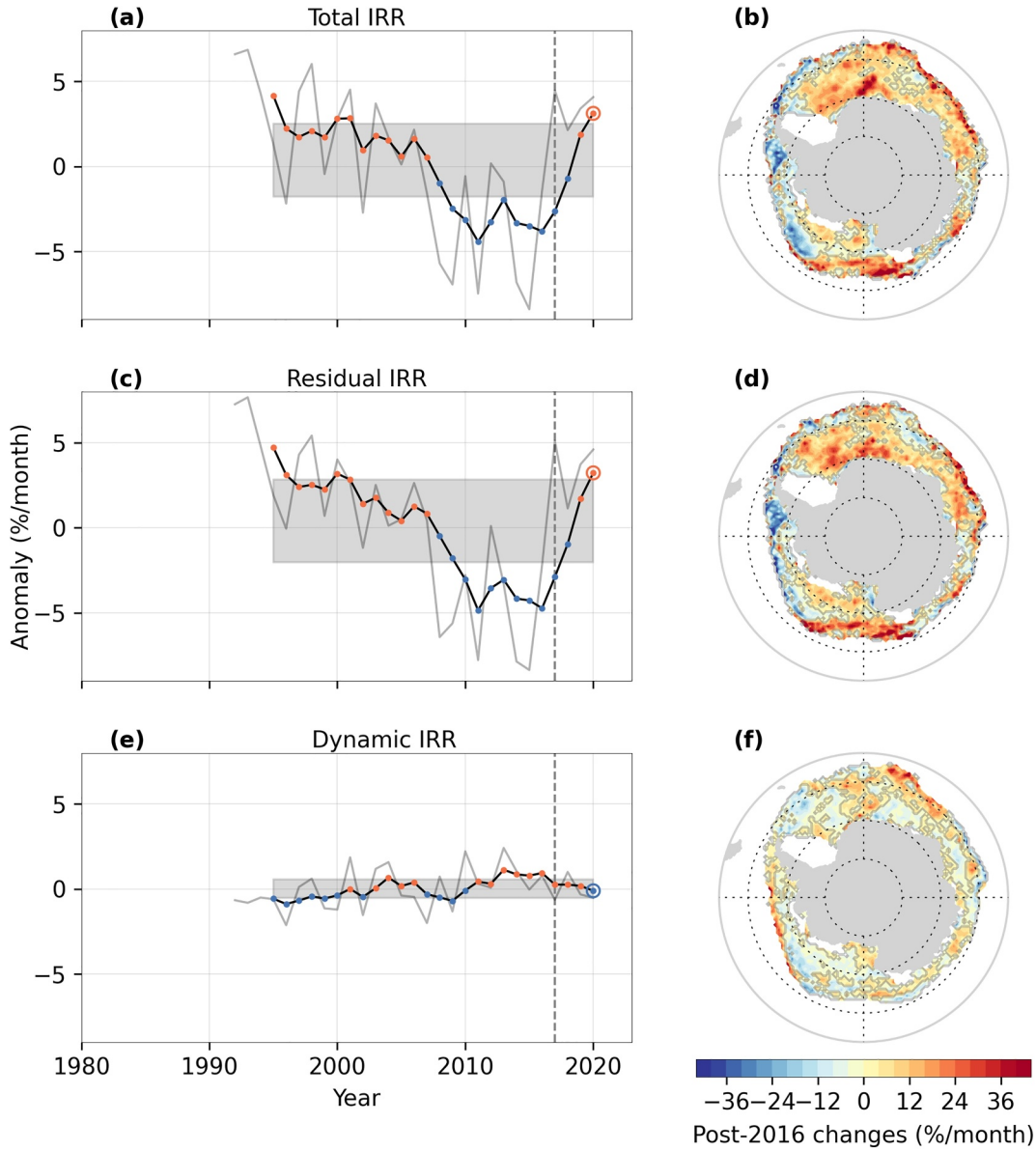


**Figure 7.** Changes in the total (a, b), residual (c, d) and dynamic (e, f) spring ice removal rate (IRR) over 1992–2020. In (a, c, and e), gray solid lines show yearly anomalies calculated as spatial mean differences over the seasonal ice zone of annual 2D fields with respect to the mean 2D field over 1992–2016. Black lines with colored dots show 4-year running mean anomalies such that the last point represent the spatial mean of the 2D fields depicted in (b), (d), and (f). 2D fields depict post-2016 changes, calculated as the differences between the 2017–2020 mean 2D fields and their pre-2016 counterpart (1992–2016). Red dots mark positive values, blue dots mark negative values and stippled gray lines mark the 2017 yearly anomalies. The gray areas delimit the mean ± the standard deviation of 4-year running mean anomalies over the whole time series. White patches in (b), (d), and (f) indicate regions out of the seasonal ice zone.

observed range of variations, whereas the simulated slope values are compatible with observational values, particularly for the thickness versus IRR and thickness versus retreat date linear relationships. The larger spread in the observations compared to the model may reflect the presence of non-ideal, non-thermodynamic drivers. Furthermore, sensitivity experiments indicate that ice-albedo feedback processes, in the sense of M. M. Holland et al. (2006), connecting solar radiation absorption through open water, basal melt of thin ice and concentration loss, are crucial to establish these relationships. First, with no loss of concentration upon basal melt (NOTIM, $p_2 = 0$), the thickness versus IRR and IRR versus retreat date relationships do not hold, as the IRR remains constant (Figures 9a and 9b). Second, with no solar absorption (NOSW, $p_1 = 0$), linear slopes of the IRR

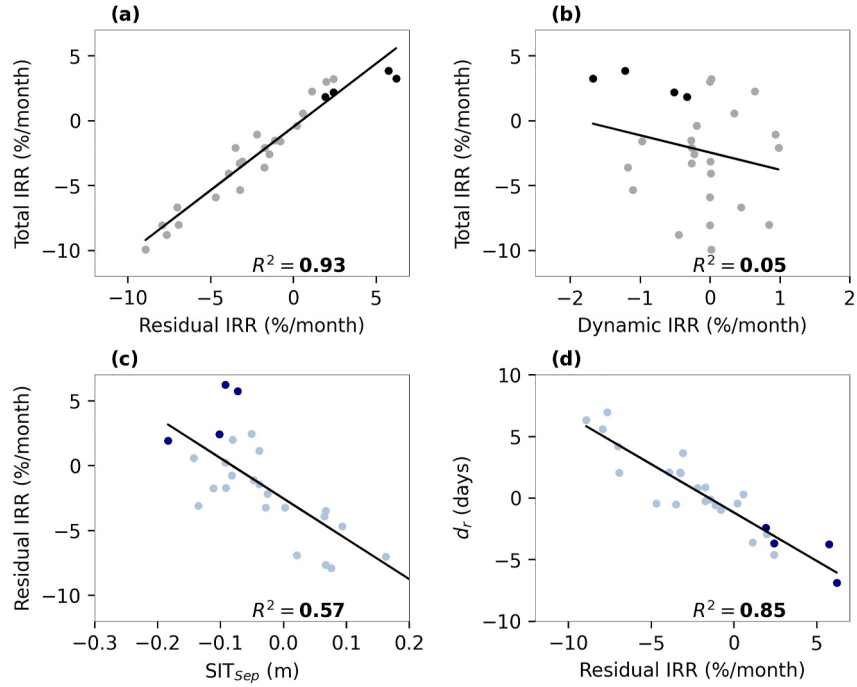


**Figure 8.** Interannual relationships between the spring sea ice removal rate (IRR) and relevant sea ice diagnostics, over 1995–2020. Detrended yearly anomalies, averaged over the seasonal ice zone, of (a), total ice removal rate (IRR) versus residual IRR, (b), total IRR versus dynamic IRR, (c), residual IRR versus September sea ice thickness ($SIT_{Sep}$) (d), retreat dates ($d_r$) versus residual IRR. The 2017–2020 anomalies are marked in dark colors. A Least Square linear regression was performed for each plot; the corresponding regression line (significant at 99%), and corresponding determination coefficient ($R^2$) are shown. The 1995–2020 period was selected to ensure consistency of the analysis, as all relevant diagnostics are available over this timeframe. Positive (negative) $d_r$ indicates later (earlier) retreat.

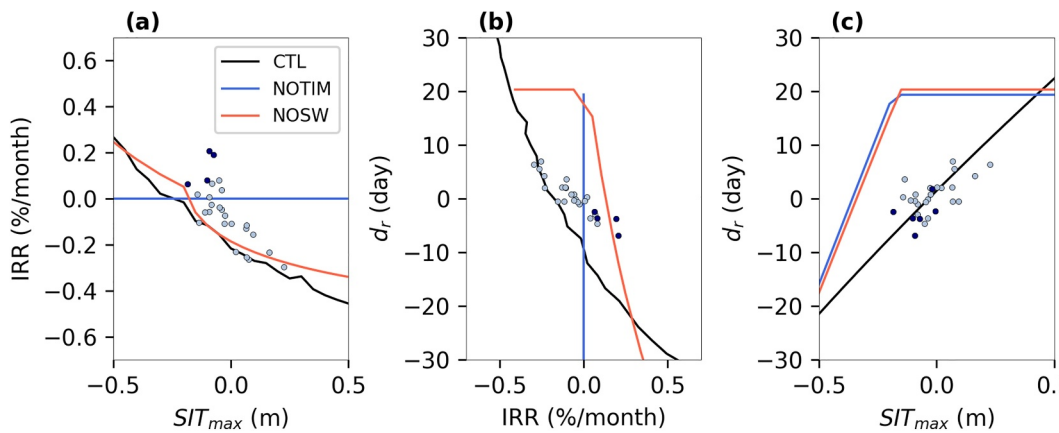


**Figure 9.** Model (lines) versus observed (symbols) relationships between (a), maximum sea ice thickness ($SIT_{max}$) and ice removal rate (IRR), (b), IRR and retreat date ($d_r$), (c), $SIT_{max}$ and $d_r$. The CTL model ensemble (black) has all processes included as described above (see Section 3). The red ensemble assumes short-wave absorption is fixed at initial value (NOSW). The blue ensemble assumes concentration does not decrease upon thickness decrease (NOTIM). Observed relationships are based on detrended anomalies over 1995–2020 for $SIT_{max}$ versus IRR and IRR versus $d_r$ relationships (as in Figures 8c and 8d), and over 1995–2022 for the $SIT_{max}$ versus $d_r$ relationship (as in Figure 6a). Observed $SIT_{max}$ is approximated by the mean September sea ice thickness. Post-2016 anomalies are marked in dark blue. Positive (negative) $d_r$ indicates later (earlier) retreat.

versus retreat date and thickness versus retreat date largely differ from observations (Figures 9b and 9c). Ultimately, these idealized simulations show that the faster melting and earlier retreat following 2016 are compatible with a thermodynamic response to ice thinning. They also highlight that ice-albedo feedback processes are crucial contributors to this response.

## 6. Discussion and Conclusion

The Antarctic sea ice season duration has undergone an unprecedented shortening since 2016 due to earlier ice retreat and later advance. These anomalies in the timing of sea ice retreat and advance are strongly linked to thinner winter sea ice, warmer summer sea surface and larger spring ice removal rate related to sea ice melt (Figure 6). Our findings indicate that the post-2016 ice season shortening is consistent with the seasonal sequence of thermodynamic processes inherent to the ice-albedo feedback, in the sense of M. M. Holland et al. (2006), in response to an initial ice thinning. According to our analysis, sea ice transport plays a comparatively minor role, consistent with previous studies highlighting that recent Antarctic sea ice changes are primarily driven by thermodynamics (Guo et al., 2023; Kimura et al., 2023).

However, some local exceptions are also visible, where ice-albedo feedback processes do not explain post-2016 changes in sea ice seasonality. First, in the Amundsen Sea, in portions of the eastern Ross Sea and along the East Antarctic coastal regions, a longer sea ice season is observed (Figures 1b and 1c). In the Amundsen and eastern Ross Seas, this lengthening mainly corresponds to a later retreat, possibly driven by southerly wind anomalies pushing sea ice (Schroeter et al., 2023) or by increased thickness (Figure 2d), but not necessarily to an earlier advance. There, sea ice changes during the advance season are more likely to be driven by sea ice advection than by thermodynamic processes, as suggested by Kimura et al. (2023). Off East Antarctica, landfast ice and polynya dynamics may contribute to the sea ice season lengthening. Therefore, for some specific regions, sea ice transport might dominate over ice-albedo feedback processes in driving the changes in sea ice seasonality following 2016.

Second, in the northwest Weddell Sea off the eastern Antarctic Peninsula, we find that the predominantly earlier retreat (Figure 2b) spatially corresponds to thicker sea ice (Figure 2d) and a decreased ice removal rate (Figure 6b), contradicting ice-albedo feedback processes. In this region, winter sea ice is thicker but less concentrated, possibly due to increased sea ice divergence (see Figure S5 in Supporting Information S1). We therefore hypothesize that during spring, the thicker ice might have a lower removal rate, and still retreat earlier due to the lower concentration at the start of the melt season. Another possible cause is that there would be a regional high bias in the satellite ice thickness retrieval. Indeed, model and altimetry-based thickness retrievals are particularly inconsistent in that region (Liao et al., 2022). Additionally, in situ sources (Worby et al., 2008), albeit sparse, do not feature a thickness maximum there.

The altimetry-based thickness product we use is fairly recent (Bocquet, 2023), and uncertainties associated with satellite observations of sea ice thickness are significant (Kacimi & Kwok, 2020; Kurtz & Markus, 2012). Therefore, the documented thickness changes carry some uncertainty, requiring cautious interpretation and independent confirmation in the future. Nonetheless, we have reasonable confidence in the thickness changes documented here. Indeed, consistent regional decreases in ice thickness have been reported in previous studies using alternative methods (Fons et al., 2023; Garnier et al., 2022). Additionally, there is spatial and temporal consistency between the observed thickness changes and well-proofed, less uncertain ice concentration variations, which is physically expected (e.g., Massonnet et al., 2013). Finally, we document a remarkable correspondence between thickness and other markers of sea ice and sea surface changes. Altogether, these elements strengthen our confidence in the observed thinning.

We next discuss potential atmospheric and oceanic changes contributing to the reduction in sea ice thickness. Enhanced southward winds as evidenced by previous studies (e.g., Nihashi & Ohshima, 2015), could increase ice divergence, thereby favoring the presence of thin newly formed ice. However, in regions of thinner sea ice (Figure 2c), the apparent increase in winter import of ice area suggests otherwise (see Figure S5 in Supporting Information S1). It is therefore more likely that the reduced ice thickness results from less growth, which can be due to changes in heat exchanges with the atmosphere and the ocean. Intensified northerly winds may increase warm air intrusions over the Southern Ocean (Schlosser et al., 2018), potentially altering the conductive flux through sea ice and reducing growth. However, increased intrusions of warm air would involve the action of several modes of atmospheric variability (e.g., Clem & Fogt, 2015), which would result in regional reductions in ice thickness rather than in the observed almost circumpolar thinning. By contrast, a near-circumpolar warming of

the subsurface ocean, as documented by several studies (Meehl et al., 2019; Purich & Doddridge, 2023; Zhang et al., 2022), could produce the observed reduction in ice thickness.

Warmer subsurface waters could potentially be entrained into the surface layer during winter, when the mixed layer reaches sufficient depth, limiting sea ice growth (Gordon, 1981; Martinson & Iannuzzi, 1998; Saenz et al., 2023; Wilson et al., 2019). Hence, a warmer subsurface ocean serves as a plausible driver of the observed reduction in sea ice thickness, more so than atmospheric changes. Nonetheless, ice-atmosphere feedbacks might amplify the effect of an ocean heat input. Thinner winter sea ice has a lower insulating power, enabling the warm underlying ocean to increase the surface air temperature, in turn leading to further sea ice thinning (Burt et al., 2016).

The cause for the subsurface warming, likely initiated around 2011 (Meehl et al., 2019; Purich & Doddridge, 2023), reaching the surface only after 2016 remains unclear. Models suggest that the persistently warm subsurface may have destabilized the mixed layer, inducing the entrainment of these warm waters into the surface (Zhang et al., 2022). However, observational evidence of this destabilization is still lacking. Ultimately, mapping hydrographic changes in the seasonal ice zone, which is beyond the scope of this work, would be required to evaluate the spatial extent of this subsurface warming and better constrain the role of the ocean in driving the recent changes in Antarctic sea ice.

## Conflict of Interest

The authors declare no conflicts of interest relevant to this study.

## Data Availability Statement

The present analyses are based on publicly available observational data. OSI-SAF sea ice concentration and drift are available from https://osi-saf.eumetsat.int/products. ESA CCI sea surface temperature is available from https://cds.climate.copernicus.eu/cdsapp#!/dataset/satellite-sea-surface-temperature?tab=overview. Sea ice thickness data is available from https://zenodo.org/records/10610697. The code for the idealized climate model is available at https://doi.org/10.6096/ctoh_sit_2023_01.

**Acknowledgments**
This research has been funded by the SCAR INSTANT research programme. S. Stammerjohn acknowledges support from the U.S. National Science Foundation Office of Polar Programs (NSF OPP-1552226 and OPP-2026045).

## References

Behrendt, A., Dierking, W., Fahrbach, E., & Witte, H. (2013). Sea ice draft in the Weddell Sea, measured by upward looking sonars. *Earth System Science Data*, *5*(1), 209–226. https://doi.org/10.5194/essd-5-209-2013

Bocquet, M. (2023). Arctic and Antarctic sea ice volume changes estimation from satellite altimetry between 1994 and 2023.

Bocquet, M., & Fleury, S. (2023). Arctic and Antarctic sea ice thickness climate data record (ERS-1, ERS-2, Envisat, CryoSat-2) [Dataset]. *Odatis*. https://doi.org/10.6096/ctoh_sit_2023_01

Burt, M. A., Randall, D. A., & Branson, M. D. (2016). Dark warming. *Journal of Climate*, *29*(2), 705–719. https://doi.org/10.1175/JCLI-D-15-0147.1

Cavalieri, D. J., & Parkinson, C. L. (2012). Arctic sea ice variability and trends, 1979-2010. *The Cryosphere*, *6*(4), 881–889. https://doi.org/10.5194/tc-6-881-2012

Clem, K. R., & Fogt, R. L. (2015). South Pacific circulation changes and their connection to the tropics and regional Antarctic warming in austral spring, 1979–2012. *Journal of Geophysical Research: Atmospheres*, *120*(7), 2773–2792. https://doi.org/10.1002/2014JD022940

Comiso, J. (2017). Bootstrap sea ice concentrations from Nimbus-7 SMMR and DMSP SSM/I-SSMIS passive microwave data, version 3. https://doi.org/10.5067/7Q8HCCWS4I0R

Comiso, J. C., Cavalieri, D. J., & Markus, T. (2003). Sea ice concentration, ice temperature, and snow depth using AMSR-E data. *IEEE Transactions on Geoscience and Remote Sensing*, *41*(2), 243–252. https://doi.org/10.1109/TGRS.2002.808317

Copernicus Climate Change Service (C3S). (2019). Sea surface temperature daily data from 1981 to present derived from satellite observations [Dataset]. *Copernicus Climate Change Service (C3S) Climate Data Store (CDS)*. https://doi.org/10.24381/cds.cf608234

EUMETSAT Ocean and Sea Ice Satellite Application Facility. (2022c). Global low resolution sea ice drift data record 1991-2020 (OSI-455; 3.0) [Dataset]. *OSI SAF FTP Server*. https://doi.org/10.15770/EUM_SAF_OSI_0012

EUMETSAT Ocean and Sea Ice Satellite Application Facility. (2022a). Global sea ice concentration climate data record 1979-2020 (OSI-450a; 3.0) [Dataset]. *OSI SAF FTP Server*. https://doi.org/10.15770/EUM_SAF_OSI_NRT_2004

EUMETSAT Ocean and Sea Ice Satellite Application Facility. (2022b). Global sea ice concentration interim climate data record 2021-2022 (OSI-430a; 3.0) [Dataset]. *OSI SAF FTP Server*. https://doi.org/10.15770/EUM_SAF_OSI_0014

Ferreira, D., Marshall, J., Bitz, C. M., Solomon, S., & Plumb, A. (2015). Antarctic Ocean and sea ice response to ozone depletion: A two-time-scale problem. *Journal of Climate*, *28*(3), 1206–1226. https://doi.org/10.1175/JCLI-D-14-00313.1

Fichefet, T., & Morales Maqueda, M. A. (1997). Sensitivity of a global sea ice model to the treatment of ice thermodynamics and dynamics. *Journal of Geophysical Research*, *102*(C6), 12609–12646. https://doi.org/10.1029/97jc00480

Fons, S., Kurtz, N., & Bagnardi, M. (2023). A decade-plus of Antarctic sea ice thickness and volume estimates from CryoSat-2 using a physical model and waveform fitting. *The Cryosphere*, *17*(6), 2487–2508. https://doi.org/10.5194/tc-17-2487-2023

Garnier, F., Bocquet, M., Fleury, S., Bouffard, J., Tsamados, M., Remy, F., et al. (2022). Latest altimetry-based sea ice freeboard and volume inter-annual variability in the Antarctic over 2003–2020. *Remote Sensing*, *14*(19), 4741. Article 19. https://doi.org/10.3390/rs14194741

Garnier, F., Fleury, S., Garric, G., Bouffard, J., Tsamados, M., Laforge, A., et al. (2021). Advances in altimetric snow depth estimates using bi-frequency SARAL and CryoSat-2 Ka–Ku measurements. *The Cryosphere*, *15*(12), 5483–5512. https://doi.org/10.5194/tc-15-5483-2021

Gordon, A. L. (1981). Seasonality of southern ocean sea ice. *Journal of Geophysical Research*, *86*(C5), 4193–4197. https://doi.org/10.1029/JC086iC05p04193

Guo, Y., Chen, X., Huang, S., & Wen, Z. (2023). Amplified interannual variation of the summer sea ice in the Weddell Sea, Antarctic after the late 1990s. *Geophysical Research Letters*, *50*(17), e2023GL104924. https://doi.org/10.1029/2023GL104924

Häkkinen, S., & Mellor, G. L. (1990). One hundred years of Arctic ice cover variations as simulated by a one-dimensional, ice-ocean model. *Journal of Geophysical Research*, *95*(C9), 15959–15969. https://doi.org/10.1029/JC095iC09p15959

Haumann, F. A., Moorman, R., Riser, S. C., Smedsrud, L. H., Maksym, T., Wong, A. P. S., et al. (2020). Supercooled southern ocean waters. *Geophysical Research Letters*, *47*(20), e2020GL090242. https://doi.org/10.1029/2020GL090242

Hersbach, H., Bell, B., Berrisford, P., Hirahara, S., Horányi, A., Muñoz-Sabater, J., et al. (2020). The ERA5 global reanalysis. *Quarterly Journal of the Royal Meteorological Society*, *146*(730), 1999–2049. https://doi.org/10.1002/qj.3803

Himmich, K., Vancoppenolle, M., Madec, G., Sallée, J.-B., Holland, P. R., & Lebrun, M. (2023). Drivers of Antarctic sea ice advance. *Nature Communications*, *14*(1), 6219. Article 1. https://doi.org/10.1038/s41467-023-41962-8

Hobbs, W., Spence, P., Meyer, A., Schroeter, S., Fraser, A. D., Reid, P., et al. (2024). Observational evidence for a regime shift in summer Antarctic sea ice. https://doi.org/10.1175/JCLI-D-23-0479.1

Holland, M. M., Bitz, C. M., Hunke, E. C., Lipscomb, W. H., & Schramm, J. L. (2006). Influence of the sea ice thickness distribution on polar climate in CCSM3. *Journal of Climate*, *19*(11), 2398–2414. https://doi.org/10.1175/JCLI3751.1

Holland, M. M., Blanchard-Wrigglesworth, E., Kay, J., & Vavrus, S. (2013). Initial-value predictability of Antarctic sea ice in the community climate system model 3. *Geophysical Research Letters*, *40*(10), 2121–2124. https://doi.org/10.1002/grl.50410

Holland, M. M., Landrum, L., Raphael, M., & Stammerjohn, S. (2017). Springtime winds drive Ross Sea ice variability and change in the following autumn. *Nature Communications*, *8*(1), 731. Article 1. https://doi.org/10.1038/s41467-017-00820-0

Holland, P. R., & Kimura, N. (2016). Observed concentration budgets of Arctic and Antarctic sea ice. *Journal of Climate*, *29*(14), 5241–5249. https://doi.org/10.1175/JCLI-D-16-0121.1

Holland, P. R., & Kwok, R. (2012). Wind-driven trends in Antarctic sea-ice drift. *Nature Geoscience*, *5*(12), 872–875. Article 12. https://doi.org/10.1038/ngeo1627

Kacimi, S., & Kwok, R. (2020). The Antarctic sea ice cover from ICESat-2 and CryoSat-2: Freeboard, snow depth, and ice thickness. *The Cryosphere*, *14*(12), 4453–4474. https://doi.org/10.5194/tc-14-4453-2020

Kimura, N., Onomura, T., & Kikuchi, T. (2023). Processes governing seasonal and interannual change of the Antarctic sea-ice area. *Journal of Oceanography*, *79*(2), 109–121. https://doi.org/10.1007/s10872-022-00669-y

Kostov, Y., Marshall, J., Hausmann, U., Armour, K. C., Ferreira, D., & Holland, M. M. (2017). Fast and slow responses of southern ocean sea surface temperature to SAM in coupled climate models. *Climate Dynamics*, *48*(5), 1595–1609. https://doi.org/10.1007/s00382-016-3162-z

Kurtz, N. T., Farrell, S. L., Studinger, M., Galin, N., Harbeck, J. P., Lindsay, R., et al. (2013). Sea ice thickness, freeboard, and snow depth products from Operation IceBridge airborne data. *The Cryosphere*, *7*(4), 1035–1056. https://doi.org/10.5194/tc-7-1035-2013

Kurtz, N. T., & Markus, T. (2012). Satellite observations of Antarctic sea ice thickness and volume. *Journal of Geophysical Research*, *117*(C8), C08025. https://doi.org/10.1029/2012JC008141

Lavergne, T., & Down, E. (2023). A climate data record of year-round global sea ice drift from the EUMETSAT OSI SAF. *Earth System Science Data Discussions*, *1–38*. https://doi.org/10.5194/essd-2023-40

Lavergne, T., Sørensen, A. M., Kern, S., Tonboe, R., Notz, D., Aaboe, S., et al. (2019). Version 2 of the EUMETSAT OSI SAF and ESA CCI sea-ice concentration climate data records. *The Cryosphere*, *13*(1), 49–78. https://doi.org/10.5194/tc-13-49-2019

Laxon, S., Peacock, N., & Smith, D. (2003). High interannual variability of sea ice thickness in the Arctic region. *Nature*, *425*(6961), 947–950. https://doi.org/10.1038/nature02050

Lebrun, M., Vancoppenolle, M., Madec, G., & Massonnet, F. (2019). Arctic sea-ice-free season projected to extend into autumn. *The Cryosphere*, *13*(1), 79–96. https://doi.org/10.5194/tc-13-79-2019

Lengaigne, M., Menkes, C., Aumont, O., Gorgues, T., Bopp, L., André, J.-M., & Madec, G. (2007). Influence of the oceanic biology on the tropical Pacific climate in a coupled general circulation model. *Climate Dynamics*, *28*(5), 503–516. https://doi.org/10.1007/s00382-006-0200-2

Liao, S., Luo, H., Wang, J., Shi, Q., Zhang, J., & Yang, Q. (2022). An evaluation of Antarctic sea-ice thickness from the Global Ice-Ocean Modeling and Assimilation System based on in situ and satellite observations. *The Cryosphere*, *16*(5), 1807–1819. https://doi.org/10.5194/tc-16-1807-2022

Libera, S., Hobbs, W., Klocker, A., Meyer, A., & Matear, R. (2022). Ocean-sea ice processes and their role in multi-month predictability of Antarctic sea ice. *Geophysical Research Letters*, *49*(8), e2021GL097047. https://doi.org/10.1029/2021GL097047

Maksym, T., & Markus, T. (2008). Antarctic Sea ice thickness and snow-to-ice conversion from atmospheric reanalysis and passive microwave snow depth. *Journal of Geophysical Research*, *113*(C2), C02S12. https://doi.org/10.1029/2006JC004085

Mallett, R. D. C., Lawrence, I. R., Stroeve, J. C., Landy, J. C., & Tsamados, M. (2020). Brief communication: Conventional assumptions involving the speed of radar waves in snow introduce systematic underestimates to sea ice thickness and seasonal growth rate estimates. *The Cryosphere*, *14*(1), 251–260. https://doi.org/10.5194/tc-14-251-2020

Manabe, S., & Stouffer, R. J. (1980). Sensitivity of a global climate model to an increase of $CO_2$ concentration in the atmosphere. *Journal of Geophysical Research*, *85*(C10), 5529–5554. https://doi.org/10.1029/JC085iC10p05529

Markus, T., & Cavalieri, D. J. (1998). Snow depth distribution over sea ice in the southern ocean from satellite passive microwave data. In *Antarctic sea ice: Physical processes, interactions and variability* (pp. 19–39). American Geophysical Union (AGU). https://doi.org/10.1029/AR074p0019

Martinson, D. G., & Iannuzzi, R. A. (1998). Antarctic Ocean-ice interaction: Implications from ocean bulk property distributions in the Weddell Gyre. In *Antarctic sea ice: Physical processes, interactions and variability* (pp. 243–271). American Geophysical Union (AGU). https://doi.org/10.1029/AR074p0243

Massom, R. A., Stammerjohn, S. E., Lefebvre, W., Harangozo, S. A., Adams, N., Scambos, T. A., et al. (2008). West Antarctic Peninsula sea ice in 2005: Extreme ice compaction and ice edge retreat due to strong anomaly with respect to climate. *Journal of Geophysical Research*, *113*(C2), C02S20. https://doi.org/10.1029/2007JC004239

Massonnet, F., Mathiot, P., Fichefet, T., Goosse, H., König Beatty, C., Vancoppenolle, M., & Lavergne, T. (2013). A model reconstruction of the Antarctic sea ice thickness and volume changes over 1980–2008 using data assimilation. *Ocean Modelling*, *64*, 67–75. https://doi.org/10.1016/j.ocemod.2013.01.003

Maykut, G. A., & McPhee, M. G. (1995). Solar heating of the Arctic mixed layer. *Journal of Geophysical Research*, *100*(C12), 24691–24703. https://doi.org/10.1029/95JC02554

Maykut, G. A., & Perovich, D. K. (1987). The role of shortwave radiation in the summer decay of a sea ice cover. *Journal of Geophysical Research*, *92*(C7), 7032–7044. https://doi.org/10.1029/JC092iC07p07032

Meehl, G. A., Arblaster, J. M., Bitz, C. M., Chung, C. T. Y., & Teng, H. (2016). Antarctic sea-ice expansion between 2000 and 2014 driven by tropical Pacific decadal climate variability. *Nature Geoscience*, *9*(8), 590–595. Article 8. https://doi.org/10.1038/ngeo2751

Meehl, G. A., Arblaster, J. M., Chung, C. T. Y., Holland, M. M., DuVivier, A., Thompson, L., et al. (2019). Sustained ocean changes contributed to sudden Antarctic sea ice retreat in late 2016. *Nature Communications*, *10*(1), 14. Article 1. https://doi.org/10.1038/s41467-018-07865-9

Meier, M. W. N. (2017). *AMSR-e/AMSR2 unified L3 daily 12.5 km brightness temperatures, sea ice concentration, motion & snow depth polar grids, version 1*. NASA National Snow and Ice Data Center Distributed Active Archive Center. https://doi.org/10.5067/RA1MIJOYPK3P

Merchant, C. J., Embury, O., Bulgin, C. E., Block, T., Corlett, G. K., Fiedler, E., et al. (2019). Satellite-based time-series of sea-surface temperature since 1981 for climate applications. *Scientific Data*, *6*(1), 223. Article 1. https://doi.org/10.1038/s41597-019-0236-x

Mezzina, B., Goosse, H., Huot, P.-V., Marchi, S., & Lipzig, N. V. (2024). Contributions of atmospheric forcing and ocean preconditioning in the 2016 Antarctic sea ice extent drop. *Environmental Research: Climate*, *3*(2), 021002. https://doi.org/10.1088/2752-5295/ad3a0b

Nihashi, S., & Ohshima, K. I. (2015). Circumpolar mapping of Antarctic coastal polynyas and landfast sea ice: Relationship and variability. *Journal of Climate*, *28*(9), 3650–3670. https://doi.org/10.1175/JCLI-D-14-00369.1

Parkinson, C. L. (1994). Spatial patterns in the length of the sea ice season in the southern ocean, 1979–1986. *Journal of Geophysical Research*, *99*(C8), 16327–16339. https://doi.org/10.1029/94JC01146

Parkinson, C. L. (2019). A 40-y record reveals gradual Antarctic sea ice increases followed by decreases at rates far exceeding the rates seen in the Arctic. *Proceedings of the National Academy of Sciences of the United States of America*, *116*(29), 14414–14423. https://doi.org/10.1073/pnas.1906556116

Parkinson, C. L., & Cavalieri, D. J. (2012). Antarctic sea ice variability and trends, 1979–2010. *The Cryosphere*, *6*(4), 871–880. https://doi.org/10.5194/tc-6-871-2012

Paul, S., Sallila, H., Hendricks, S., & Rinne, E. (2021). ESA CCI+ climate change initiative phase 1, D2.1 sea ice thickness algorithm theoretical basis document (ATBD), v.3.1. Retrieved from https://climate.esa.int/en/projects/sea-ice/Sea-Ice-Key-Documents/

Perovich, D. K., Light, B., Eicken, H., Jones, K. F., Runciman, K., & Nghiem, S. V. (2007). Increasing solar heating of the Arctic Ocean and adjacent seas, 1979–2005: Attribution and role in the ice-albedo feedback. *Geophysical Research Letters*, *34*(19), L19505. https://doi.org/10.1029/2007GL031480

Purich, A., & Doddridge, E. W. (2023). Record low Antarctic sea ice coverage indicates a new sea ice state. *Communications Earth & Environment*, *4*(1), 314. Article 1. https://doi.org/10.1038/s43247-023-00961-9

Raphael, M. N., & Handcock, M. S. (2022). A new record minimum for Antarctic sea ice. *Nature Reviews Earth & Environment*, *3*(4), 215–216. Article 4. https://doi.org/10.1038/s43017-022-00281-0

Saenz, B. T., McKee, D. C., Doney, S. C., Martinson, D. G., & Stammerjohn, S. E. (2023). Influence of seasonally varying sea-ice concentration and subsurface ocean heat on sea-ice thickness and sea-ice seasonality for a 'warm-shelf' region in Antarctica. *Journal of Glaciology*, *69*(277), 1466–1482. https://doi.org/10.1017/jog.2023.36

Schlosser, E., Haumann, F. A., & Raphael, M. N. (2018). Atmospheric influences on the anomalous 2016 Antarctic sea ice decay. *The Cryosphere*, *12*(3), 1103–1119. https://doi.org/10.5194/tc-12-1103-2018

Schroeter, S., O'Kane, T. J., & Sandery, P. A. (2023). Antarctic sea ice regime shift associated with decreasing zonal symmetry in the Southern Annular Mode. *The Cryosphere*, *17*(2), 701–717. https://doi.org/10.5194/tc-17-701-2023

Simpkins, G. R., Ciasto, L. M., & England, M. H. (2013). Observed variations in multidecadal Antarctic sea ice trends during 1979–2012. *Geophysical Research Letters*, *40*(14), 3643–3648. https://doi.org/10.1002/grl.50715

Smith, A., Jahn, A., & Wang, M. (2020). Seasonal transition dates can reveal biases in Arctic sea ice simulations. *The Cryosphere*, *14*(9), 2977–2997. https://doi.org/10.5194/tc-14-2977-2020

Stammerjohn, S., Martinson, D. G., Smith, R. C., Yuan, X., & Rind, D. (2008). Trends in Antarctic annual sea ice retreat and advance and their relation to El Niño–Southern Oscillation and Southern Annular Mode variability. *Journal of Geophysical Research*, *113*(C3), C03S90. https://doi.org/10.1029/2007JC004269

Stammerjohn, S., Massom, R., Rind, D., & Martinson, D. (2012). Regions of rapid sea ice change: An inter-hemispheric seasonal comparison. *Geophysical Research Letters*, *39*(6), L06501. https://doi.org/10.1029/2012GL050874

Stuecker, M. F., Bitz, C. M., & Armour, K. C. (2017). Conditions leading to the unprecedented low Antarctic sea ice extent during the 2016 austral spring season. *Geophysical Research Letters*, *44*(17), 9008–9019. https://doi.org/10.1002/2017GL074691

Thorndike, A. S., Rothrock, D. A., Maykut, G. A., & Colony, R. (1975). The thickness distribution of sea ice. *Journal of Geophysical Research*, *80*(33), 4501–4513. https://doi.org/10.1029/JC080i033p04501

Turner, J., Holmes, C., Caton Harrison, T., Phillips, T., Jena, B., Reeves-Francois, T., et al. (2022). Record low Antarctic sea ice cover in February 2022. *Geophysical Research Letters*, *49*(12), e2022GL098904. https://doi.org/10.1029/2022GL098904

Turner, J., Phillips, T., Marshall, G. J., Hosking, J. S., Pope, J. O., Bracegirdle, T. J., & Deb, P. (2017). Unprecedented springtime retreat of Antarctic sea ice in 2016. *Geophysical Research Letters*, *44*(13), 6868–6875. https://doi.org/10.1002/2017GL073656

Vancoppenolle, M., Timmermann, R., Ackley, S. F., Fichefet, T., Goosse, H., Heil, P., et al. (2011). Assessment of radiation forcing data sets for large-scale sea ice models in the southern ocean. *Deep Sea Research Part II: Topical Studies in Oceanography*, *58*(9–10), 1237–1249. https://doi.org/10.1016/j.dsr2.2010.10.039

Vivier, F., Hutchings, J. K., Kawaguchi, Y., Kikuchi, T., Morison, J. H., Lourenço, A., & Noguchi, T. (2016). Sea ice melt onset associated with lead opening during the spring/summer transition near the North Pole. *Journal of Geophysical Research: Oceans*, *121*(4), 2499–2522. https://doi.org/10.1002/2015JC011588

Wilson, E. A., Riser, S. C., Campbell, E. C., & Wong, A. P. S. (2019). Winter upper-ocean stability and ice–ocean feedbacks in the sea ice–covered southern ocean. *Journal of Physical Oceanography*, *49*(4), 1099–1117. https://doi.org/10.1175/JPO-D-18-0184.1

Worby, A. P., Geiger, C. A., Paget, M. J., Van Woert, M. L., Ackley, S. F., & DeLiberty, T. L. (2008). Thickness distribution of Antarctic sea ice. *Journal of Geophysical Research*, *113*(C5), C05S92. https://doi.org/10.1029/2007JC004254

Zhang, L., Delworth, T. L., Yang, X., Zeng, F., Lu, F., Morioka, Y., & Bushuk, M. (2022). The relative role of the subsurface southern ocean in driving negative Antarctic sea ice extent anomalies in 2016–2021. *Communications Earth & Environment*, *3*(1), 302. Article 1. https://doi.org/10.1038/s43247-022-00624-1

## Erratum

The originally published version of this article contained a typographical error in the caption for Figure 3. Specifically, "(a) Ice season duration" should be changed to "(c) Ice season duration and " and "1980–2016 for (c)" should be corrected to "1980–2016 for (a–c)." The updated caption should read as follows: "Post-2016 changes in (a) retreat date, (b) advance date, (c) ice season duration, (d) September sea ice thickness (SIT), and (e) maximum sea surface temperature (SST). Changes are calculated as differences between the 2017–2022 mean 2D fields and their pre-2016 counterparts. The reference period for pre-2016 conditions depends on data availability: 1980–2016 for (a–c); 1995–2016 for (d); and 1983–2016 for (e). White patches indicate regions outside the seasonal ice zone." The error has been corrected, and this may be considered the authoritative version of record.